

Time-resolved spectroscopy of the visible emission band in strontium titanate

R. Leonelli* and J. L. Brebner

Département de Physique, Université de Montréal, Montréal, Québec, H3C 3J7 Canada

(Received 2 October 1985)

The luminescence spectrum of SrTiO₃ from 1.6 to 3.2 eV has been studied as a function of time elapsed after excitation. A broad emission band with maximum intensity at 2.44 eV can be observed. The shape of this band, including some fine structure, can be reproduced by the Huang-Rhys model for excitation-lattice interaction. A vibron energy $\hbar\Omega = 88$ meV and a Huang-Rhys factor $S_0 \approx 6$ are deduced. It is shown that those values are consistent with what is required for exciton self-trapping. The luminescence intensity has been followed for times between 100 ns and 10 ms. The decay curves indicate that two recombination processes are involved. We associate the first one with self-trapped excitons interacting with acoustic phonons and the second with the retarded formation of self-trapped excitons from localized electrons and holes. The emission appears to be quenched by a nonradiative recombination channel whose activation energy is 0.07 eV.

I. INTRODUCTION

SrTiO₃ is a polar material which crystallizes in the ABO₃ perovskite structure, where *A* is a group-I-II element and *B* is a transition metal. Absorption spectra¹ indicate that SrTiO₃ has an indirect gap whose energy at 77 K is 3.27 eV. The flatness of the conduction band in the Γ -*X* direction^{2,3} and the presence of strong electron-phonon coupling make SrTiO₃ a good candidate in which to observe polaronic effects in optical⁴ and transport measurements.^{5,6}

When pure crystals of SrTiO₃ are excited by radiation above the band gap in energy, a broad greenish luminescence band appears whose intensity decreases rapidly when the temperature is raised above about 50 K.⁷⁻¹² Since this band could not be related to the presence of any impurity or defect, it was proposed to attribute it to exciton self-trapping.¹⁰ However, intensity decay curves follow a power-law behavior typical of bimolecular processes¹² which are usually extrinsic in nature. In order to better understand the mechanisms involved in the generation of the emission band, we have performed time-resolved luminescence measurements on nominally pure crystals of SrTiO₃.

In the next section we describe the experimental conditions. The measurements are detailed in Sec. III and discussed in Sec. IV. We ascribe the emission spectra to the recombination of self-trapped excitons (STE's). Within the Huang-Rhys model of excitation-lattice interaction, we have obtained estimations for the lattice "vibron" energy and for the excitation-lattice coupling factor. The luminescence intensity decay curves are analyzed with a model involving both mono- and bimolecular processes. At times shorter than 10 μ s, the decay is observed to follow a $t^{-\eta}e^{-t/\tau}$ law which corresponds to the radiative annihilation of STE's directly formed by the free carriers of the excited crystal. The preexponential factor can be explained in terms of an interaction between the self-trapped exciton and acoustic phonons if a piezoelectriclike coupling is assumed. At longer times, the decay follows a power law. We attribute this behavior to the retarded for-

mation of STE's from localized electrons and holes. We present a numerical method to obtain distributions of decay times from measured decay curves. The influence of sample temperature is also discussed. Conclusions are drawn in the final section.

II. EXPERIMENTAL

Nominally pure single crystals of SrTiO₃ were obtained from NL Industries. Several samples were examined and two were selected which gave the most intense emission. These two samples were from different boules and their dimensions were 4.0 \times 6.0 \times 0.40 mm³ for sample 1 and 5.0 \times 5.0 \times 0.21 mm³ for sample 2. The samples were polished to optical quality, then etched in 85 vol % phosphoric acid at 120 °C for 10 min. The room-temperature resistivity of the platelets was in the vicinity of 10¹² Ω cm for both samples. With an electronic mobility of about 0.1 cm² V⁻¹ s⁻¹ (Ref. 6), this gives a free-carrier equilibrium concentration of less than 5 \times 10⁸ cm⁻³. Analysis by mass spectrometry usually reveals several parts per million of impurities, mostly Al³⁺ and Fe³⁺ substituting for the Ti⁴⁺ ions.¹³ Charge compensation then requires about one-half the same number of oxygen vacancies.

The samples were mounted in the helium gas chamber of a Janis Super-Varitemp cryostat. The sample temperature was measured with a calibrated germanium resistor and was varied between 4.2 and 50 K by means of a Lakeshore Cryotronics temperature controller. The crystals were illuminated by 3-ns pulses generated by a Lumonics 861S laser operating at 20 Hz with a nitrogen-helium gas mixture. The laser emission, at 3.68 eV, is 0.4 eV above the band gap of SrTiO₃. The intensity of the exciting beam was kept below 1.0 mJ cm⁻² to prevent crystal damage.

The luminescence of sample 1 was collected in a right-angle geometry in order to maximize the signal-to-noise ratio, whereas sample 2 was studied in a straight-through geometry. The emitted light was focused onto the slits of a Jobin-Yvon HR-320 spectrometer having an aperture of

$f/4.2$, and detected by a Hamamatsu R955 photomultiplier. The spectral response of the optical system including the focusing mirrors was carefully measured using a calibrated source, and used to correct the raw data.

For time delays following excitation shorter than $50 \mu\text{s}$, the signal was captured by a Tektronix 7912 AD digitizer and, for longer times, by a Tektronix 7D20 digitizer. The overall time resolution of the setup was less than 1 ns. It was possible either to set the spectrometer at a fixed wavelength and to measure the luminescence intensity as a function of the time elapsed since the excitation pulse, or to vary the wavelength and to measure the signal integrated over an appropriate time window for time-resolved spectra. The experiment was controlled by an Apple II Plus microcomputer. The data could also be transferred to a mainframe computer for detailed analysis.

III. RESULTS

A. Emission spectra

Emission spectra obtained from both samples at liquid-helium temperature are presented in Fig. 1. For these spectra, the photomultiplier signal was integrated from 0.5 to $1.0 \mu\text{s}$ after excitation. We reported earlier that these spectra are independent of the time-integration window.¹² The luminescence band, which is non-Gaussian in form, has a maximum at 2.44 eV, which is 0.73 eV below the band gap. The spectra from sample 1 show a regular structure on the low-energy side with a

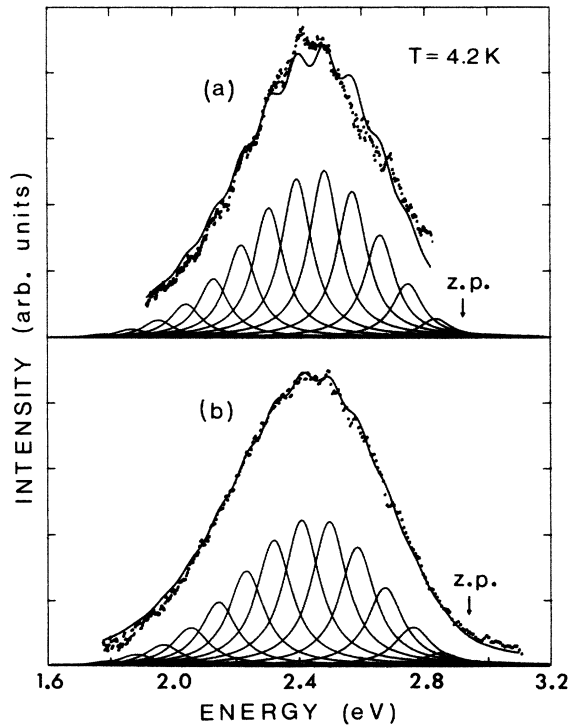


FIG. 1. Visible emission spectra of SrTiO_3 at 4.2 K for (a) sample 1 and (b) sample 2. The dots represent the luminescence intensity integrated from 0.5 to $1.0 \mu\text{s}$ after excitation. The solid lines show the fit obtained using the theory described in the text.

periodicity of about 90 meV. This is a good indication that the emission comes from a single electronic level interacting strongly with the lattice, as can be seen by the following arguments.

The Hamiltonian of the system can be written as¹⁴

$$H = H_{\text{ex}} + H_{\text{lat}} + H_{\text{ex-lat}}, \quad (1)$$

where H_{ex} is the excitation part of the Hamiltonian and where H_{lat} and $H_{\text{ex-lat}}$, respectively, the lattice and the excitation-lattice parts, are given by

$$H_{\text{lat}} = \frac{1}{2} \hbar \Omega (P^2 + Q^2), \quad (2)$$

$$H_{\text{ex-lat}} = -\kappa Q. \quad (3)$$

Q and P are generalized coordinates and κ is a coupling factor. If κ is strong enough, the excitation is trapped in a parabolic lattice potential. The lattice vibrations are quantized, with level separation $\hbar \Omega$ (also called vibron energy). Within the Huang-Rhys model,¹⁵ the probability of a transition from the lowest level of the excited state $n'=0$ to any level of the fundamental state n follows a Poisson distribution. The emission band for $kT \ll \hbar \Omega$ is then given by

$$P(E) = \text{const} \times e^{-S_0} \sum_{n=0}^{\infty} \frac{S_0^n}{n!} A_n(E), \quad (4)$$

where S_0 , the Huang-Rhys factor, is

$$S_0 = \frac{1}{2} \left[\frac{\kappa}{\hbar \Omega} \right]^2, \quad (5)$$

and where $A_n(E)$ describes the spread in energy of each individual transition. If lifetime effects are predominant, $A_n(E)$ can be described by a Lorentzian:

$$A_n(E) = \frac{1}{\pi} \frac{\Gamma/2}{(E_0 - E - n\hbar\Omega)^2 + (\Gamma/2)^2}. \quad (6)$$

Here E_0 is the zero-phonon transition energy; that is, the energy between the $n'=0$ and $n=0$ levels.

The least-squares fit of the emission spectra of sample 1 with Eqs. (4)–(6) is represented in Fig. 1(a) by a solid line. The parameters thus deduced are listed in Table I. Also shown in Fig. 1 are the individual peaks $A_n(E)$ ($n=0-12$). The arrow indicates the position of the zero-phonon (z.p.) transition. Given the simplicity of the Hamiltonian, the agreement between the model and the experimental data is quite good.

The solid line in Fig. 1(b) also represents a similar

TABLE I. Parameters of the Huang-Rhys model obtained from a least-squares fit of the experimental data.

	Sample No.	
	1	2
S_0	5.7 ± 0.1	6.1 ± 0.1
E_0 (eV)	2.92 ± 0.01	2.94 ± 0.01
$\hbar \Omega$ (eV)	0.088 ± 0.004	0.088^a
Γ (eV)	0.12 ± 0.01	0.14 ± 0.01

^aFixed parameter.

least-squares fit, but with $\hbar\Omega$ kept fixed at the value of 88 meV, deduced from the spectrum of sample 1. As can be seen from Table I, a slight increase of the Huang-Rhys factor S_0 and of the half-width Γ is sufficient to smear out the structure in Fig. 1(b).

B. Luminescence decay

The intensity of the luminescence as a function of time elapsed after excitation is shown for both samples in Fig. 2. Two different decay processes can be observed on such curves. The first one is more apparent at low enough excitation intensity and is exemplified by the decay curve of sample 2 with an excitation density E_{exc} of $30 \mu\text{J cm}^{-2}$ (Fig. 2, curve B, open circles). We have previously shown¹² that this process can be well represented by the empirical law

$$I_1(t) = \frac{A_1}{(1+t/b)^\beta}. \quad (7)$$

When the excitation density exceeds about $100 \mu\text{J cm}^{-2}$, a second decay process becomes apparent as a shoulder which first decreases according to a power law, then disappears in a way consistent with an exponential decay (Fig. 2, curve B, solid circles at times shorter than $100 \mu\text{s}$). For reasons explained in Sec. IV B, we have chosen to represent this second decay process by the function

$$I_2(t) = A_0 t^{-\eta} e^{-t/\tau}. \quad (8)$$

Two types of curves were observed at high excitation intensities, depending on the specific sample under study. To the first one belongs curve B of Fig. 2. It can be reproduced well by the trial function

$$I_A(t) = I_1(t) + I_2(t). \quad (9)$$

Curve A of Fig. 2 belongs to the second type, where the transition between the two decay processes is smooth so that a fit with Eq. (9) gives poor results in the intermediate region around $100 \mu\text{s}$. A better trial function was

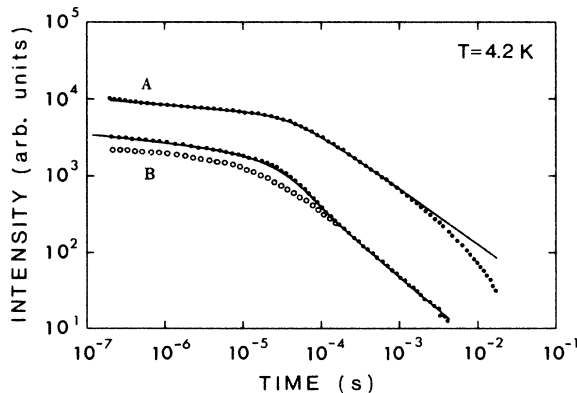


FIG. 2. Log-log plot of the luminescence decay curves in response to a 3-ns-long uv laser pulse. Curve A, sample 1; curve B, sample 2. \circ , $E_{\text{exc}} = 30 \mu\text{J cm}^{-2}$; \bullet , $E_{\text{exc}} = 130 \mu\text{J cm}^{-2}$. The solid lines show the fit obtained using Eq. (10) with the parameters of Table II.

TABLE II. Parameters in Eq. (10) obtained from a least-squares fit of the experimental data.

	Sample no.	
	1	2
τ (μs)	20	26
η	0.10	0.12
A_1	0.99	0.57
b (μs)	45	26
β	0.73	0.88

found to be the sum of I_2 with a convolution of I_1 and I_2 ; that is

$$I_B(t) = A_0 \left[t^{-\eta} e^{-t/\tau} + A_1 \int_0^{t-\epsilon} (t-t')^{-\eta} \times e^{-(t-t')/\tau} \left[1 + \frac{t'}{b} \right]^{-\beta} dt' \right], \quad (10)$$

with $\epsilon \ll t$. The solid lines in Fig. 2 are a best fit of the experimental data using Eq. (10). Satisfactory agreement is obtained for both curves with the parameters given in Table II. It is to be noted that $I_B(t)$ has the same asymptotic behavior in the short- and long-time limits and the same number of parameters as $I_A(t)$. The fact that I_B reproduces the observed data better suggests that the excitation whose recombination yields the luminescence through the fast decay $I_2(t)$ is the end product of the process described by $I_1(t)$.

The variation of the decay curves with temperature is given in Fig. 3. The numbers at the right of the curves indicate their temperatures in K. The intensity of the curves relative to each other has been arbitrarily fixed.

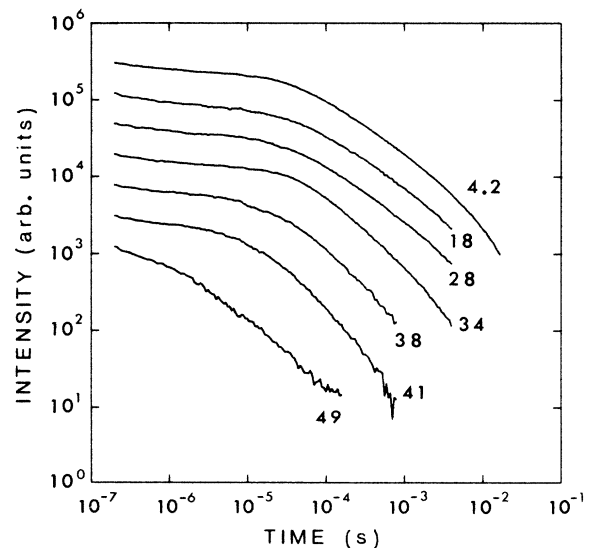


FIG. 3. Log-log plot of the luminescence decay curves of sample 1 at different temperatures. The numbers on the right are the temperatures in K.

IV. DISCUSSION

A. Emission band

A broad luminescence in the blue-green region of the visible spectrum is often observed in compounds containing diluted titanate octahedra. For example, $\text{La}_2\text{MgSn}_{1-x}\text{Ti}_x\text{O}_6$, a material with perovskite structure, emits in the blue-green and the violet regions.¹⁶ In $\text{BaZr}_{1-x}\text{Ti}_x(\text{PO}_4)_2$, a broad emission centered at 2.4 eV can be observed for values of x as low as 0.05, whereas no such emission occurs in $\text{BaZr}(\text{PO}_4)_2$ (Ref. 17). An emission at 2.25 eV with a half-width of 0.76 eV is seen in fluorophosphate glasses in which inserted titanium atoms are found in an octahedral environment of fluorine and oxygen atoms.¹⁸

In all these compounds, the interatomic interactions within the titanate octahedra are stronger than in the rest of the matrix. Such is not the case in SrTiO_3 , and therefore a broad-band emission cannot occur in this material unless the translational symmetry is broken. Symmetry breaking could arise from the presence of impurity atoms or oxygen vacancies in the neighborhood of an emitting center. However, in SrTiO_3 , the emission is enhanced with increasing crystal purity.^{7,8} Moreover, a very similar emission is observed in x-ray-excited BaTiO_3 which rapidly decreases with the introduction of a few percent of iron impurities.¹⁹

It therefore appears that the emission is intrinsic in origin in SrTiO_3 and corresponds to the recombination of a self-trapped exciton (STE). Several arguments can be made concerning the existence of STE's in a given material. First, the energy gained by self-trapping has to be less than the energy lost because of the localization of the exciton. This requires²⁰

$$S_0 \hbar\Omega > \nu J, \quad (11)$$

where ν is the number of nearest neighbors (six for SrTiO_3) and J is the nearest-neighbor exchange energy.

A question now arises about the structure of the STE. The band-structure calculations of Kahn and Leyendecker,² in agreement with optical measurements,¹ indicate that the electron is the heavy carrier in SrTiO_3 . Moreover, photoconductivity experiments⁹ show that the visible luminescence efficiency is determined mainly by the hole traffic towards localized electrons. One can thus assume that the self-trapping comes mostly from the interaction between the lattice and the electronic part of the exciton and take for J the value found for small electronic polarons,⁶ e.g., $J \approx 0.1$ eV. Equation (11) is therefore nearly satisfied.

Another argument involves the Urbach tail often seen in the absorption spectra of polar materials. It is characterized by an absorption coefficient α that follows

$$\alpha = \alpha_0 \exp \left[\sigma \frac{(E - E_g)}{T} \right], \quad (12)$$

with $E < E_g$. As shown by Toyozawa,^{20,21} such an exponential tail can arise from an excitation-lattice interaction strong enough to induce momentary self-trapping of

excitons. Numerical calculations²² have indicated that a stable STE state becomes favored if the Urbach coefficient σ satisfies

$$\sigma < \frac{s}{1 - \frac{1}{2\nu}}, \quad (13)$$

where $S = 1.5$ in direct-band-gap materials and $s = 0.85$ in indirect-band-gap materials. In the latter case, Eq. (13) requires that $\sigma < 0.93$ for SrTiO_3 . Capizzi and Frova¹ have found values for σ in the range 0.84–1.03, depending on temperature. Although the occurrence of STE's cannot be ascertained by the above arguments, it nevertheless appears plausible.

The above-mentioned model, according to which the STE in SrTiO_3 is constituted from an electron trapped within a strong lattice deformation surrounded by a fairly delocalized hole, is substantiated by the value of $\hbar\Omega$ (88 meV, Table I) slightly lower than the value of the LO phonon with the strongest Frölich coupling coefficient (99 meV, Ref. 4). A reduction in the same proportions has been observed for polaron absorption in AgBr, where $\hbar\Omega = 15$ meV and $\hbar\omega_{\text{LO}} = 17$ meV (Ref. 23), and in NaCl:F, where $\hbar\Omega = 30$ meV and $\hbar\omega_{\text{LO}} = 34$ meV (Ref. 24). It follows that in SrTiO_3 the electron–LO-phonon interaction is not screened very much by the surrounding hole, so that the exciton wave function has to extend over several elementary cells.

The differences in the shape of the two emission bands shown in Fig. 1 can probably be explained by an increased density of crystal defects or impurities in sample 2 as compared to sample 1. As indicated in Ref. 20, the perturbing potential of the defects can act so as to effectively increase the coupling coefficient κ of Eq. (3), or reduce the stiffness of the lattice and hence the vibron energy $\hbar\Omega$. Both effects would result in an increased value of the Huang-Rhys factor S_0 . As seen from Table I and Fig. 1, a variation of less than 10% in S_0 is sufficient to smear out in sample 2 the structure seen in sample 1.

B. Luminescence decay

The elements presented in the preceding sections converge to attribute the visible emission band to self-trapped excitons. However, instead of an expected exponential law, a careful examination of the decay curves reveal that both exponential and power-law decays are present, depending on the excitation conditions (Fig. 2). Such a behavior is usually associated with extrinsic processes.^{25,26} Nevertheless, given the very low mobility of the electronic polarons in SrTiO_3 , the above observations can be reconciled with an interpretation which attributes the emission to the annihilation of a self-trapped exciton, as summarized in Fig. 4. Some of the electrons promoted to the conduction band by the absorption of a uv photon from the pump laser form small polarons (channel 3 in Fig. 4). The polarons interact with holes trapped near crystal defects or impurities (channel 1) and form an intermediate state: the STE (channels 4 and 5). The recombination of these STE's results in the slowly decaying luminescence tail described by the convolution of $I_1(t)$ and $I_2(t)$ [second part of the right-hand side of Eq. (10)]. The pro-

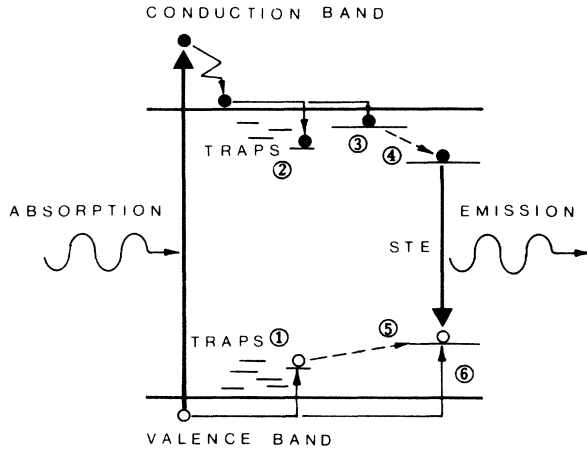


FIG. 4. Schematic of the luminescence processes in SrTiO₃. 1, hole capture; 2, electron capture; 3, small-polaron formation; 4 and 5, retarded formation of a STE; 4 and 6, direct formation of a STE.

cesses involving electrons trapped by crystal defects do not have to be considered here. They result in competing channels which effectively reduce the visible emission efficiency. If the excitation intensity is high enough, the hole traps are saturated and the STE's are formed directly (channels 4 and 6), giving rise to the faster near-exponential decay [first part of the right-hand side of Eq. (10)]. Both processes are further detailed below.

1. Slow decay

The interaction between localized electrons and holes can be described in terms of a reaction involving two populations with density N_A and N_B . Following Blumen *et al.*,²⁷ we write the reaction kinetics as

$$N_A(t) + C = N_B(t), \quad (14)$$

$$\frac{dN_A(t)}{dt} = -K(t)N_A(t)N_B(t), \quad (15)$$

where $K(t)$ is the recombination rate and C is a constant. In the monomolecular regime, the density of one of the species, say B , is much greater than the density of the other. (B can also designate the density of states in the continuum.) The solution of Eqs. (14) and (15) is then

$$N_A(t) = N_A(0) \exp \left[-C \int_0^t K(t') dt' \right], \quad (16)$$

which results in an exponential decay if K is independent of time.

On the other hand, if $N_A(0) = N_B(0)$, the solution is

$$\frac{1}{N_A(t)} = \frac{1}{N_A(0)} + \int_0^t K(t') dt'. \quad (17)$$

This is the bimolecular regime. If the recombination rate K is independent of time, it follows from Eq. (17) that the luminescence decay curve is given by the decay law $I_1(t)$ [Eq. (7)], with $\beta=2$. In the more general case, the probability of recombination between localized species depends on the explicit spatial distribution and K is a function of

time. This problem has been extensively treated in the literature, but to our knowledge, no analytic solution has been proposed. Nevertheless, the empirical law $I_1(t)$, with the exponent β lying between 0.5 and 2, is approximately valid over several decades in time in high-gap materials with luminescent centers,^{10,25,28} in semiconductors with random distribution of donors and acceptors,²⁹ and in amorphous semiconductors.³⁰

2. Fast decay

At times shorter than 100 μ s, the luminescence follows a near-exponential behavior which we associate with the radiative annihilation of STE's formed directly by electrons and holes in the conduction and valence bands.

This decay deviates at short times from the expected exponential law but rather follows a power law $t^{-\eta}$. Since η is of the order of 0.1, the deviation is small, but it is nevertheless well within the resolution of our measurements. In order to explain this deviation, we tentatively propose that an infrared divergent behavior of low-energy lattice excitations interacting with the STE occurs in SrTiO₃. Infrared divergence was recently introduced in relation with radiative recombination in amorphous chalcogenides,³¹ where the function

$$I(t) \propto -\frac{d}{dt} \left\{ \exp \left[- \left(\frac{t}{\tau} \right)^\eta \right] \right\} \quad (18)$$

could successfully reproduce the observed luminescence decay.

This function is somewhat different from Eq. (8). It was, however, derived in the specific context of the dielectric response in disordered systems³² and it is not obvious that it should be directly applied to excitonic recombination. It is more appropriate to go back to the initial formalism proposed by Mahan.³³ One can write that the probability of emission per unit time from an electronic level interacting with a continuum of lattice states is

$$I_2(t) \propto \exp \{ -\text{Re}[\phi(t)] \}, \quad (19)$$

where

$$\phi(t) = i\Sigma t + \theta(t). \quad (20)$$

In Eq. (20), Σ is the self-energy of the excitation whose lifetime is deduced from $\text{Im}(\Sigma)$ and $\theta(t)$ is given at $T=0$ K by

$$\theta(t) = \int_0^\infty \frac{|\gamma(\omega)|^2}{\omega^2} \rho(\omega) (1 - e^{-i\omega t}) d\omega. \quad (21)$$

Here, $\rho(\omega)$ is the density of lattice states and $\gamma(\omega)$ is the coupling coefficient. We believe that in SrTiO₃ these lattice states are simply acoustic phonons. The density of states is then proportional to ω^2 for small ω . If some part of γ behaves as

$$\gamma(\omega) \propto \omega^{-1/2}, \quad (22)$$

the number of excited phonons in a given transition diverges.^{32,33} One can nevertheless evaluate $\theta(t)$ by introducing a cutoff frequency ω_c such that $\omega_c t \gg 1$. One then obtains

$$\theta(t) = \eta[\gamma_E + \ln(it\omega_c) + E_1(it\omega_c)], \quad (23)$$

where γ_E is the Euler constant and $E_1(x)$ is a Euler polynomial with negligible value for $|x| \gg 1$. It follows from Eqs. (20), (21), and (23) that $I_2(t)$ has the form given by Eq. (8).

In the case of SrTiO₃, the exciton-acoustic-phonon interaction appears mediated by crystal defects, since the coefficient η is correlated to crystal quality, ranging from less than 0.1 in the better samples to about 0.2 in samples with more lattice defects.¹¹ It is also interesting to note that the experimentally determined value of η is slightly higher in sample 2 than in sample 1 (see Table II), as was the Huang-Rhys factor S_0 .

The coupling coefficient γ given by Eq. (22) corresponds to the form used to describe the interactions between electrons and acoustic phonons in piezoelectric crystals.³⁴ The question arises as to the possibility of such a coupling in SrTiO₃, which has a centrosymmetric structure. An explanation can be found in the behavior of the ferroelectric soft mode in SrTiO₃. This mode corresponds to the displacement of the titanium and strontium atoms along a cubic axis, which creates an electric dipole moment.⁴ In BaTiO₃, a phase transformation occurs in which this mode "freezes out." The crystal becomes ferroelectric and hence piezoelectric. In SrTiO₃, the free energy corresponding to the Ti atom lying in the center position is always lower than that for the Ti atom lying above or below the center position of the octahedron and the ferroelectric phase is never reached. However, when the ferroelectric mode softens, as it does as the temperature is lowered, it becomes easier for the Ti atom to spend some time in the metastable off-center position.

Piezoelectric regions could then develop at low enough temperatures, eventually pinned down by crystal defects.

C. Temperature evolution

The data shown in Fig. 3 cannot be straightforwardly analyzed by fitting the curves with Eq. (10), first because the visible emission efficiency decreases as the temperature is raised and hence the precision of the data becomes insufficient, and second because more complex processes probably also take place. In order to extract some information from the data shown in Fig. 3, it is more useful to introduce a distribution of decay times $G(\tau)$, defined as the probability that a pair of interacting species recombines with an effective lifetime τ . If the duration of the exciting laser pulse is much smaller than any time τ considered, the distribution function is related to the luminescence intensity by³⁵

$$I(t) = \text{const} \times \int_0^\infty \frac{G(\tau)}{\tau} e^{-t/\tau} d\tau. \quad (24)$$

The inverse relation is

$$G(\tau) = \text{const} \times \frac{1}{\tau} \Phi \left[\frac{1}{\tau} \right], \quad (25)$$

where $\Phi(x)$ is the inverse Laplace transform of $I(t)$. In order to evaluate $\Phi(x)$, we have made use of the Gaver-Stehfest algorithm:³⁶

$$\Phi_n(x) = \frac{\ln(2)}{x} \sum_{j=1}^n V_j \left[\frac{j}{x} \ln(2) \right], \quad (26)$$

with

$$V_j = (-1)^{n/2+j} \sum_{k=(j+1)/2}^{\min(j, n/2)} \frac{k^{n+2}(2k)!}{(n/2-k)!k!(k-1)!(j-k)!(2k-j)!}. \quad (27)$$

This algorithm gives satisfactory values of the inverse Laplace transform of most analytic functions with n less than 10.³⁷

The actual decay curves of Fig. 3 were smoothed and interpolated by third-order collocation polynomials. Due to amplification of experimental uncertainties, the Gaver-Stehfest algorithm could only be used with $n=4$. Nevertheless, tests on analytic trial functions showed that the coarse features of the inverse Laplace transform were well represented. The derived form of the distributions $G(\tau)$ corresponding to the decay curves are presented in Fig. 5. It was not possible to identify the origin of the fine structure seen at short times, since its width corresponds to the resolution of the algorithm. The broad structure at longer times is assigned to the distribution of the decay times of the localized species. The peak position of this broad structure, indicated by an arrow, moves towards shorter times as the temperature is increased. This peak corresponds to the most probable decay time τ_r .

If one assumes that there is a competing nonradiative recombination process which has an activation energy E_a , one can write

$$\tau_r = \frac{\tau_R}{(1 + \tau_R \nu_{NR} e^{-E_a/kT})}, \quad (28)$$

where τ_R is some radiative lifetime and ν_{NR} is the nonradiative transition rate. The values of τ_r as a function of temperature are plotted in Fig. 6 as points. The solid line is the least-squares fit of Eq. (28). The optimized parameters are $\tau_R = 52 \mu\text{s}$, $\nu_{NR} = 1.2 \times 10^{13} \text{ s}^{-1}$, and $E_a = 0.070 \text{ eV}$.

One can see that, although crude, the above method of analysis gives informations consistent with what has been obtained otherwise. The radiative lifetime τ_R is not far from the parameter b of Eq. (10) found for the same sample at $T = 4.2 \text{ K}$ ($45 \mu\text{s}$, Table II). The activation energy E_a is nearly the same as the one obtained from the visible

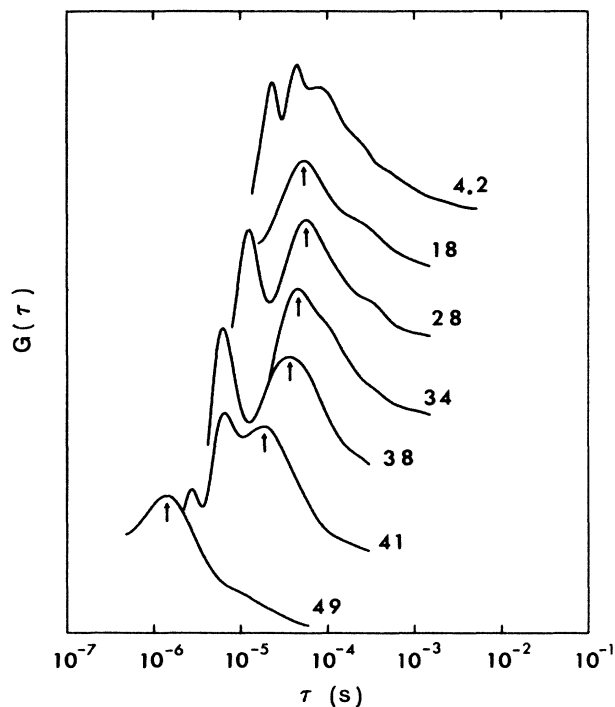


FIG. 5. Distribution of decay times obtained from a numerical evaluation of the inverse Laplace transform of the decay curves shown in Fig. 3. The numbers on the right are the temperatures in K.

luminescence band intensity in BaTiO₃ (0.08 eV, Ref. 19). We could not determine whether the activated competing nonradiative process involved is intrinsic or extrinsic in origin.

V. CONCLUSIONS

We have studied the visible broad emission band in SrTiO₃ in detail. This band is assumed to be excitonic in origin since it is observed in many compounds containing titanate octahedra and cannot be associated with any particular impurity. The agreement between the observed band shape and what is predicted on the basis of the Huang-Rhys model indicates that the emission is accompanied by strong lattice relaxation. The vibronic levels involved in the excitation transition are separated by an energy $\hbar\Omega = (88 \pm 4)$ meV and the Huang-Rhys factor S_0 has a value of about 6. The small variations of S_0 for different samples can be attributed to the presence of crystal defects. The values of the vibron energy and the Huang-

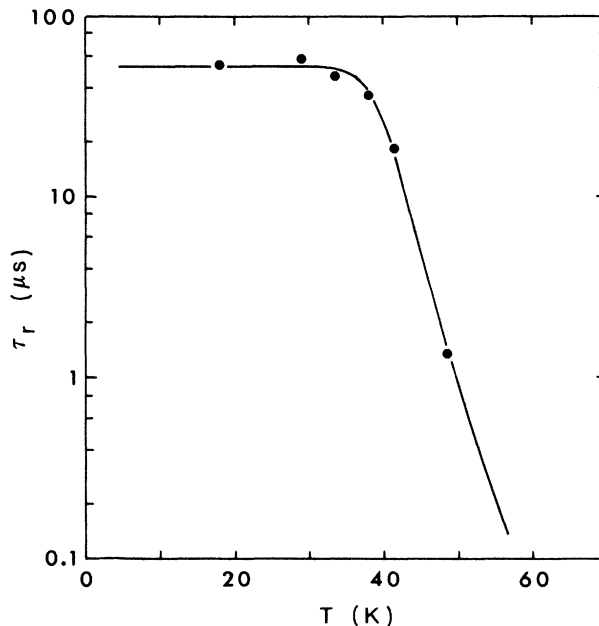


FIG. 6. Evolution of the peak of the distribution of decay times as a function of temperature. The solid lines show the fit obtained using Eq. (28).

Rhys factor are consistent with what is required for exciton self-trapping, according to the theory developed by Toyozawa.²⁰

Time-resolved measurements show that both mono- and bimolecular processes are involved. The experimental data can be well explained by a model in which the electrons form small polarons while the holes interact with the polarons to form self-trapped excitons, either immediately or after being trapped for a certain time by impurities. The recombination rate of the STE is not constant, but rather leads to the decay law $t^{-\eta}e^{-t/\tau}$. We tentatively explain the preexponential factor in terms of an infrared-divergent behavior of acoustic phonons interacting with the self-trapped exciton. The evolution of the decay curves with temperature indicates that the emission is quenched by a competing nonradiative channel which has an activation energy of 0.07 eV.

ACKNOWLEDGMENTS

This research was supported by the Natural Sciences and Engineering Research Council of Canada and by the Fonds pour la formation de chercheurs et l'aide à la recherche (Ministère de l'Éducation du Québec).

*Present address: Laboratoire de spectroscopie et d'optique du corps solide, 5, rue de l'Université, 67000 Strasbourg, France.

¹M. Capizzi and A. Frova, Phys. Rev. Lett. **25**, 1298 (1970); Nuovo Cimento B **5**, 181 (1971).

²A. H. Kahn and A. J. Leyendecker, Phys. Rev. **135**, A1321 (1964).

³L. F. Mattheiss, Phys. Rev. B **6**, 4718 (1972); P. Pertosa and F.

M. Michel-Calendini, *ibid.* **17**, 2011 (1978).

⁴J. L. Brebner, S. Jandl, and Y. Lépine, Phys. Rev. B **23**, 3816 (1981).

⁵G. Perluzzo and J. Destry, Can. J. Phys. **54**, 1482 (1976).

⁶D. Kéroack, Y. Lépine, and J. L. Brebner, J. Phys. C **17**, 833 (1984).

⁷L. Grabner, Phys. Rev. **177**, 1315 (1965).

- ⁸Y. T. Sihvonen, *J. Appl. Phys.* **38**, 4431 (1967).
- ⁹T. Feng, *Phys. Rev. B* **25**, 627 (1982).
- ¹⁰M. Aguilar and F. Agullo-Lopez, *J. Appl. Phys.* **53**, 9009 (1982).
- ¹¹R. Leonelli and J. L. Brebner, *J. Lumin.* **31&32**, 96 (1984).
- ¹²R. Leonelli and J. L. Brebner, *Solid State Commun.* **54**, 505 (1985).
- ¹³F. J. Morin and J. R. Oliver, *Phys. Rev. B* **8**, 5847 (1973).
- ¹⁴See, for example, R. Englman, *Non-Radiative Decay of Ions and Molecules in Solids* (North-Holland, Amsterdam, 1980).
- ¹⁵D. Curie, in *Optical Properties of Ions in Solids*, edited by B. Di Bartolo (Plenum, New York, 1975).
- ¹⁶A. J. H. Macke, *Phys. Status Solidi A* **39**, 117 (1977).
- ¹⁷G. Blasse, *Struct. Bonding* (Berlin) **42**, 19 (1980).
- ¹⁸Gan Fuxi and Liu Huiming, *J. Lumin.* **31&32**, 348 (1984).
- ¹⁹M. Aguilar, G. Gonzalo, and G. Godefroy, *Solid State Commun.* **30**, 525 (1979).
- ²⁰Y. Toyozawa, in *Relaxations of Elementary Excitations*, edited by R. Kubo and E. Hanamura (Springer-Verlag, Berlin, 1980).
- ²¹H. Sumi and Y. Toyozawa, *J. Phys. Soc. Jpn.* **31**, 342 (1971).
- ²²M. Schreiber and Y. Toyozawa, *J. Phys. Soc. Jpn.* **51**, 1544 (1982); **52**, 318 (1983).
- ²³R. C. Brandt and F. C. Brown, *Phys. Rev.* **181**, 1241 (1969).
- ²⁴F. Carlier and G. Jacobs, *Phys. Status Solidi B* **89**, 193 (1978).
- ²⁵W. L. Medlin, *Phys. Rev.* **122**, 837 (1961).
- ²⁶P. J. Dean, J. D. Cuthbert, and R. T. Lynch, *Phys. Rev.* **179**, 754 (1969).
- ²⁷A. Blumen, J. Klafter, and G. Zumofen, *Phys. Rev. B* **27**, 3429 (1983).
- ²⁸C. J. Delbecq, D. L. Dexter, and P. H. Yuster, *Phys. Rev. B* **17**, 4765 (1978).
- ²⁹D. G. Thomas, J. J. Hopfield, and W. M. Augustyniak, *Phys. Rev.* **140**, A202 (1965).
- ³⁰R. A. Street, *Adv. Phys.* **30**, 593 (1981).
- ³¹K. L. Ngai and K. Murayama, *Physica* **117&118B**, 980 (1983); K. Murayama and T. Ninomiya, *Solid State Commun.* **53**, 125 (1985).
- ³²K. L. Ngai, *Comments Solid State Phys.* **9**, 127 (1979); **9**, 141 (1980).
- ³³G. D. Mahan, in *Solid State Physics: Advances in Research and Applications*, edited by F. Seitz, D. Turnbull, and H. Ehrenreich (Academic, New York, 1974), Vol. 29, p. 75.
- ³⁴E. I. Rashba, in *Excitons*, edited by E. I. Rashba and M. D. Sturge (North-Holland, Amsterdam, 1982).
- ³⁵C. Tsang and R. A. Street, *Phys. Rev. B* **19**, 3027 (1979).
- ³⁶H. Stehfest, *Commun. ACM* **13**, 47 (1970).
- ³⁷B. Davies and B. Martin, *J. Comput. Phys.* **33**, 1 (1979); R. G. Jacquot, J. W. Steadman, and C. N. Rhodine, *IEEE Circ. Syst. Mag.* **5**, 4 (1983).